

Gaussian Process Regression as a Sustainable Data-driven Background Estimate Method at the (HL)-LHC

Jackson Barr^{1,2} and Bingxuan Liu³

¹Centre for Data Intensive Science and Industry, University College London

²Deutsches Elektronen-Synchrotron DESY

³School of Science, Shenzhen Campus of Sun Yat-sen University

Abstract

In this article, we evaluate the performance of a data-driven background estimate method based on Gaussian Process Regression (GPR). A realistic background spectrum from a search conducted by CMS is considered, where a large sub-region below the trigger threshold is included. It is found that the L_2 regularisation can serve as a set of hyperparameters and control the overall modelling performance to satisfy common standards established by experiments at the Large Hadron Collider (LHC). In addition, we show the robustness of this method against increasing luminosity via pseudo-experiments matching the expected luminosity at the High-Luminosity LHC (HL-LHC). While traditional methods relying on empirical functions have been challenged during LHC Run 2 already, a GPR-based technique can offer a solution that is valid through the entire lifetime of the (HL)-LHC.

Keywords

Gaussian Process/ Data Science / BSM Physics/ Large Hadron Colliders

Contents

1	Introduction	3
2	Test Dataset	4
3	Model Setup	4
4	Background Estimate Validation	6
5	Sensitivity Study	7
6	Robustness in HL-LHC	11
7	Summary	15
A	Impacts of the L_2 regularisation	15
	References	16

1 Introduction

Background modelling plays a pivotal role in high energy experiments in both searches for new physics [1–3] and precision measurements of the standard model [4, 5]. Thanks to the careful tuning and calibrations, simulated event samples can describe the data at the required level of precision for most cases. However, certain processes, such as multijet, produced through the strong interactions of quarks and gluons, are known to be suboptimal in the simulation. Quite often, we need to up-weight the simulation of multijet in certain kinematic regions due to its extremely large cross-section, resulting in significant statistical uncertainties. In addition, the theoretical uncertainties are not sufficient to ensure desired precision across the entire phase space [6–13]. To overcome this challenge, various experiments have developed data-driven methods to estimate the multijet background in physics analyses. In the pursuit of heavy particles with narrow widths, i.e., analyses looking for bumps, a common background estimate strategy is to apply a functional fit to the data spectrum. An empirical function is able to fit the background distribution, which is smoothly falling, while a narrow peak over the background cannot be incorporated into the function. A widely used function has the following form:

$$f(x) = p_0(1 - x)^{p_1} x^{p_2 + p_3 \ln x + p_4 (\ln x)^2 + \dots}$$

where x is a scaled variable defined as $x = m_{jj}/\sqrt{s}$. Variations of the above function are also viable options [14–17]. Depending on how large and how complex the dataset is, one can decide how many higher order logarithmic terms to include. Exponential functions and Bernstein polynomials have been applied in analyses as well [18–20].

This methodology has been quite successful, but the unprecedented integrated luminosity recorded by the LHC starts challenging it. In fact, several recent analyses reported that this function family can not easily incorporate the large datasets any more. Therefore, ATLAS developed a sliding window technique where individual fit is performed for each bin using a subset of the spectrum [14, 15]. In addition to the increasing luminosity, the expanding search programme also demands a more universal strategy not relying on empirical functions. Naturally, the community has started re-thinking about the functional fit approach and investigating completely alternative methodologies.

In ref. [21], a method based on orthonormal series is constructed, and it is successfully applied in an ATLAS analysis as the primary background estimate [22]. It does not rely on empirical functional forms, and it is mathematically sound. With a complete orthonormal basis, an arbitrary spectrum can be described as long as there are enough terms. Though it is more general compared to the canonical functional fit, the authors of ref. [21] had to come up with a new basis that is more suitable for HEP experiments. The new method developed in ref. [23] uses symbolic regression to automate parametric modelling, which shows great flexibility as well. Methods in ref. [21] and ref. [23] are both parametric in their final applications.

Gaussian Process Regression (GPR), on the other hand, is a non-parametric technique widely used in machine learning and statistics [24]. A Gaussian Process is a collection of random variables such that any finite combination of them have a joint Gaussian distribution. Its potential usage in HEP experiments is discussed in ref. [25, 26] and several LHC results have applied this method to achieve various goals, such as template smoothing [27, 28] or background estimation [16, 29]. In a GPR, the bin contents $\nu_1 \dots \nu_n$ are described by a Gaussian PDF:

$$p(\nu_i; \mu_i, K) = \frac{1}{\sqrt{(2\pi)^N |K|}} \exp \left(-\frac{1}{2} \sum_{i,j} (\nu_i - \mu_i) K_{ij}^{-1} (\nu_j - \mu_j) \right),$$

where the μ_i 's are the bin means and K is the covariance matrix, which is parameterised by a kernel function $K(x_i, x_j)$. A common choice of kernel is the Radial Basis Function (RBF) kernel:

$$K(x_i, x_j) = \exp\left(-\frac{\|x_i - x_j\|}{2\ell^2}\right),$$

where, ℓ is the length scale of the kernel. It determines how closely correlated neighbouring points are and can be fit to data through maximising the marginal likelihood of the observations. The authors of ref. [25] and ref. [26] explored the application of GPR in dijet resonance searches. While previous work was concentrated on testing different kernels, in this work, we demonstrate that the L_2 regularization can be introduced as a set of hyperparameters to control the overall performance of GPR. Applying the widely adopted RBF kernel, with minimal hyperparameter tuning, GPR is capable of fitting a complicated spectrum that is challenging for functional fit methods. It is also robust against the increasing luminosity up to the HL-LHC era.

The article is organised as follows: Section 2 details the test datasets in this work; Section 3 discusses the optimal representation of the data and the GPR model setup; Section 5 lays out a comprehensive study of the expected sensitivity, followed by a similar study in the context of the HL-LHC in Section 6; and finally, Section 7 gives a summary.

2 Test Dataset

The majority of published resonance searches consider a smoothly falling background. To ensure no local features are introduced by the trigger selection, the low-mass regions are often not used, abandoning a sizeable amount of data. There have been attempts to include the whole dataset, such as a search for b -tagged resonances conducted in CMS [30]. In this search, the m_{jj} spectrum is divided into three regions, with each region fitted by a different function, because there are no proper single functions that can describe the entire spectrum. One clear advantage of GPR is the ability to handle complex spectra; hence, this work selects this analysis and uses its published data to construct the test dataset. A large set of pseudo-experiments is generated for the statistical tests, using the smooth background provided in ref. [30]. Each pseudo-dataset is achieved by varying the event count in every bin independently according to a Poisson law. Figure 1 shows the seed template used to generate the pseudo-data and one example dataset. The signal injection tests mentioned in Section 5 are generated similarly after the signal events are added to the background.

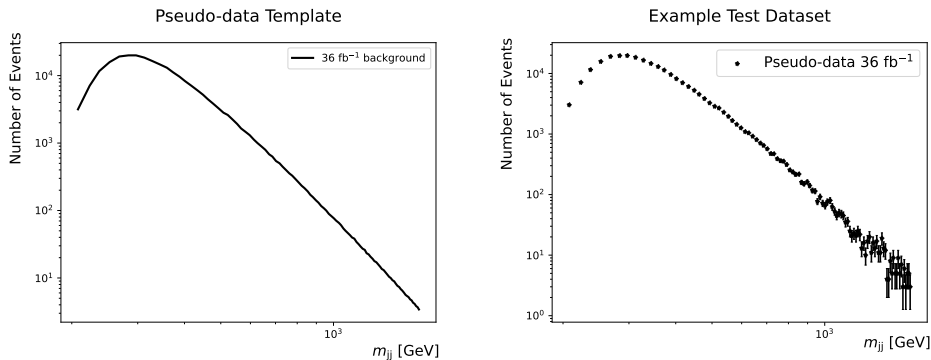


Figure 1: The smooth template used to generate the pseudo-datasets (left) and one of the example pseudo-datasets (right), representing the LHC scenario.

3 Model Setup

This work utilises the GPR module available in SCIKIT-LEARN 1.3.0, without any modifications to the core libraries.

3.1 Data Pre-processing

The dataset used for resonance searches in the hadronic final states is often very sizeable. In this work, we use a binned dataset, so for each mass point (x) there is the corresponding number of entries (y). Its rapidly falling nature and the large mass coverage require a proper pre-processing step. Applying the logarithms of x and y can achieve both fast convergence and good performance. Figure 2 shows an example regulated background dataset and hypothetical gaussian-like signal events given different mass and width parameters. The signal is well contained within an approximately 0.5 interval on the x -axis, so the lower bound of the length scale is set to 0.5.

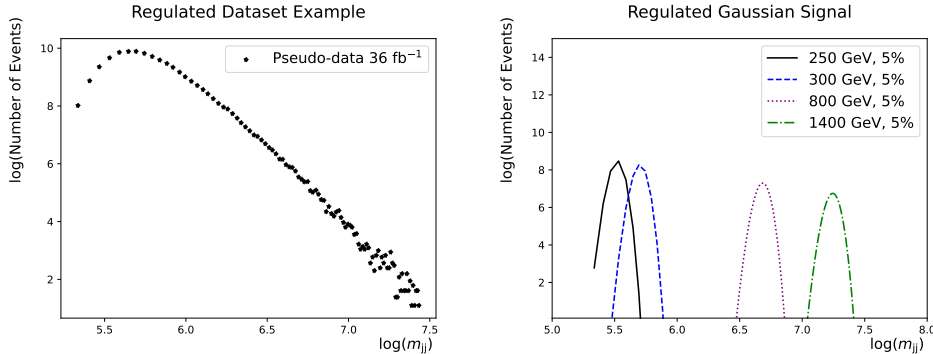


Figure 2: An example of the pre-processed background-only pseudo-datasets (left) and an illustration of the distributions for the 5% gaussian-like signal at the 250, 300, 800 and 1400 GeV mass points (right).

3.2 Kernel Selection

The kernel choice has a significant impact on the performance. As already mentioned in Section 1, there is a large series of kernels to choose from [25, 26]. The goal of this work is not to find or construct the most optimal kernel, but to demonstrate the generality of a GPR-based method. Therefore, we use the multiplication of the two most common ones, an RBF and a constant kernel: $C(c) \times \text{RBF}(\ell)$. The bounds for c and ℓ have to be selected carefully. Especially when ℓ becomes too small, there is a risk of overfitting that leads to signal absorption. It is because a localised feature like a narrow signal will increase the correlation between neighbouring points in the region where it is located.

3.3 Regularisation

In the functional fit method, users have a set of criteria, such as what is listed in Section 4. When a function cannot satisfy this list, usually the first reaction is to find a better-performing one. Similarly, we can also try to craft a more suitable customised kernel in a GPR-based strategy, but it is not the purpose of this study. In fact, this problem can be addressed differently, by biasing the minimisation to satisfy the imposed standards.

L_2 regularisation, is a well-known method to apply such biases [31]. The core idea is the addition of a diagonal matrix to the covariance matrix, so each point in the dataset will have its corresponding biasing term. This regularisation is realised in SCIKIT-LEARN via the α array, whose length is the same as that of the input data. In regions where the data points are highly correlated and known to be incompatible with the rest, the corresponding elements in the α array are decreased, which can improve the performance. Since the model predicts y given x , this regularisation is only applied to the x -axis. The α array is effectively a set of hyperparameters to tune. The nominal is set to $\alpha_i = \sqrt{y_i}/(y_i \log y_i)$, which is the relative uncertainty of $\log y_i$ propagated from y_i .

3.4 Hyperparameters

Table 1 summarises the hyperparameters and their nominal values. The lower bound on the RBF length scale is motivated by Figure 2 as discussed before, while the upper bound is set to 20, which is more than three times larger than the width of the spectrum. The bounds on the constant kernel are set to an arbitrarily large or small number, allowing it to float freely. α_i is optimised further by a set of multiplication factors, f_i , in Section 4, to satisfy the performance criteria.

Table 1: A list of hyperparameters of the GPR model.

Name	Explanation	Nominal Values
ℓ_0	RBF kernel length scale bound lower bound	0.5
ℓ_1	RBF kernel length scale bound higher bound	20
c_0	constant kernel lower bound	10^{-5}
c_1	constant kernel lower higher bound	10^{18}
α_i	diagonal elements added to the kernel matrix	$\sqrt{y_i}/(y_i \log y_i)$
f_i	multiplication factors applied to α_i	1

4 Background Estimate Validation

The performance of background estimation based on a functional fit is assessed via widely used goodness-of-fit tests, such as the reduced χ^2 test [32]. In addition, the Kolmogorov–Smirnov (KS) test evaluates how compatible the residual is with a normal distribution [33], as it is expected when the background estimate is unbiased. Though these two classic tests reveal the quality of the overall performance, they cannot detect local biases efficiently. As the search strategy is designed to find narrow peaks, such mis-modelling is likely to induce false-positive errors.

The false-positive rates can be quantified via pseudo-experiments. Naturally, the criterion depends on the specific statistical test adopted by the analysis. In this study, we consider a model-agnostic method named ‘‘Bump Hunter’’ (BH), which calculates the probability for the largest deviation between observation and expectation to originate from statistical fluctuations [34]. The corresponding mass interval is also identified. The p -values reported from pseudo-experiments considering background-only test datasets are expected to be flat if the background estimate is unbiased. A PYTHON implementation of this algorithm, PYBUMP HUNTER [35], is used.

It is found that shrinking f_i associated with the mass bins before the smoothly falling region improves the precision in the corresponding m_{jj} region. A coarse scan using fewer pseudo-experiments indicates that once f_i below 320 GeV is reduced to 0.1, the performance becomes stable. Table 2 summarises the test results from the nominal setup and the one where the first eleven f_i -s are set to 0.1 ($f_{1-11} = 0.1$), a configuration randomly selected among the tested ones where up to the first fifteen f_i -s are scaled. The latter case achieves much better performance in all three tests. Furthermore, as seen in Figure 3, the BH p -values are homogeneously distributed as expected. Figure 4 illustrates the performance difference in one of the pseudo-experiments.

Though the background modelling has passed the above tests, there can still be remaining biases that need to be taken into account as the uncertainties. Such residual biases are observed in Figure 5, summarising the most significant BH intervals. The predominant cluster near 250 GeV in the nominal case is mitigated largely by changing f_{1-11} to 0.1, but those two clusters localised near 400 and 500 GeV are still visible. There is plenty of freedom to tune f_i further, but the rest of the work uses this benchmark setup.

Table 2: Summary of the fit performance for the nominal f_i and setting f_{1-11} to 0.1.

	Nominal	$f_{\alpha}^{1-11} = 0.1$
KS p-value > 0.05	86%	88%
$\chi^2/n\text{DoF} < 1.5$	65%	85%
BH p-value > 0.1	51%	87%

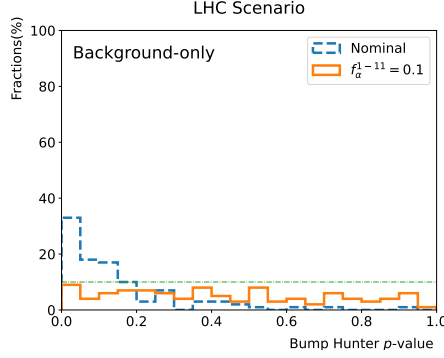


Figure 3: BH p -value distributions of 100 background-only pseudo-experiments in the LHC condition, for the nominal setup (dashed line) and $f_{1-11} = 0.1$ (solid line).

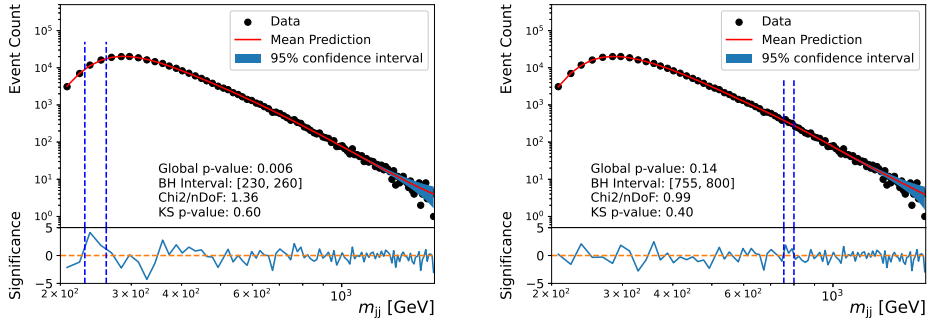


Figure 4: Comparison between an example background-only pseudo-dataset (solid point) and the background estimate from GPR (solid line), for the nominal setup (left) and $f_{1-11} = 0.1$ (right). The vertical dashed lines indicate the boundaries of the most significant deviation reported by BH.

5 Sensitivity Study

Previously, we have identified a configuration that gives us acceptable background modelling precision in the background-only case. This section will demonstrate that this configuration retains good sensitivity to signals across the entire spectrum. When it comes to analyses using data-driven background estimate methods, we have to check carefully how robust the method is against the presence of signal events. It is evaluated by a series of signal injection tests. A gaussian-like signal with a width of 5% is used as a benchmark signal hypothesis. Four mass points are included to cover various locations in the spectrum. The 250 GeV point is below the trigger threshold, and the 300 GeV point is right at the plateau. These regions are often discarded in physics analyses. The 1400 GeV point is close to the end of the m_{jj} distribution, while the 800 GeV point is in the middle of the smoothly falling region where optimal

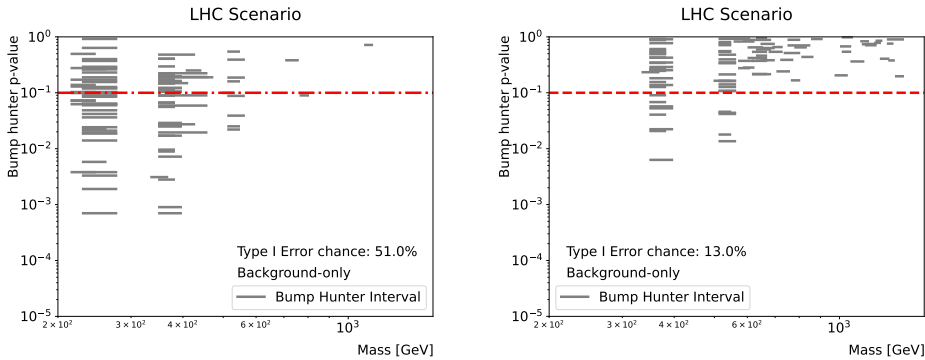


Figure 5: Summary of the BH p -values and the corresponding mass intervals (solid horizontal segments), for the nominal setup (left) and $f_{1-11} = 0.1$ (right). The horizontal dashed line corresponds to a critical value of 0.1.

sensitivity is expected when a traditional functional fit strategy is applied.

The amount of signal events injected is quantified by s/\sqrt{b} in a given m_{jj} window centred at the signal mass, covering 68.3% of the signal events. Table 3 lists the injection tests conducted. One hundred test datasets are prepared for each scenario and then fed into the sensitivity evaluation procedure as detailed in the next section.

Table 3: Summary of the signal injection tests.

Mass [GeV]	Width	Strength
250	5%	10,15
300	5%	7,10
800	5%	5,7
1400	5%	5,7

5.1 Sensitivity Evaluation

The sensitivity of a search should be evaluated with the full analysis chain executed. There exist a number of metrics to quantify the sensitivity, such as the expected exclusion limits for given BSM hypotheses. Both the CMS and ATLAS analyses often offer model-independent results using the BH algorithm, which reports a global p -value indicating how likely the most significant deviation observed comes from background fluctuations [34]. The signal injection test can be done using pseudo-experiments where the probability of reporting a p -value below the threshold is examined for a given amount of signal events injected. The p -value threshold is chosen to be 0.1 in the signal injection test as well. As shown in Figure 6, the sensitivity is optimal for the region in the middle with sizeable sidebands on both sides to constrain the background estimate, and it drops when moving towards the end of the spectrum. The performance is reduced even more in the low mass region below (on) the plateau.

Figure 7 presents the chance of successfully reporting a p -value less than 0.1 in the correct mass region where the signal events are injected. It is noticed that when injecting a 300 GeV signal, there is a high chance of reporting a significant deviation at the wrong location. It is related with the residual bias near 400 GeV seen in Figure 5. Figure 8 shows random examples of the pseudo-experiments that have successfully reported a p -value below 0.1, with the BH intervals marked as well.

The 250 GeV signal point is very close to the starting of the mass spectrum, with no constraints from the sideband on the low mass side, so the sensitivity is naturally degraded. Figure 6 reveals that the

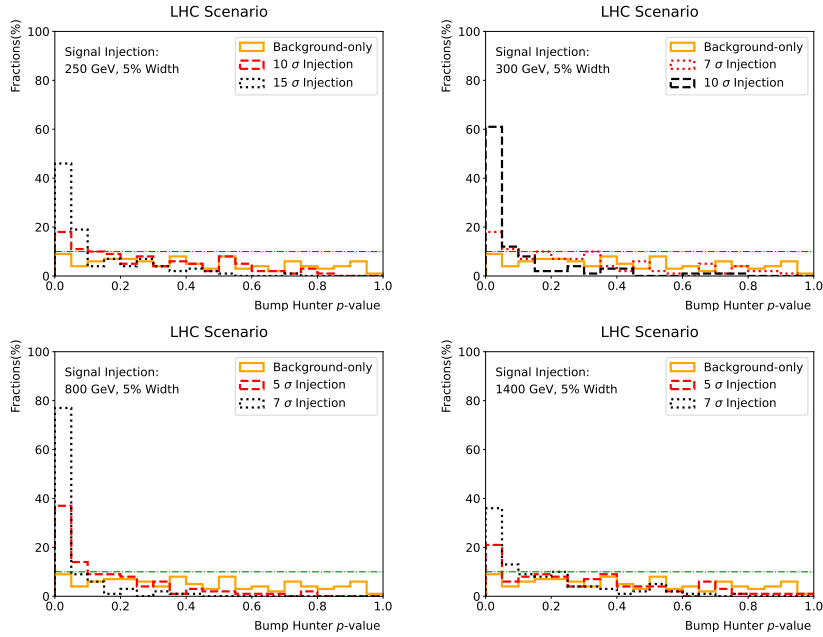


Figure 6: Summary of BH p -values obtained in the signal injection tests, for the 250 GeV (upper-left), 300 GeV (upper-right), 800 GeV (lower-left) and 1400 GeV (lower-right) signal mass points.

probability of reporting p -values below 0.1 only starts to increase visibly when more than ten times of s/\sqrt{b} signal events are injected. Though this behaviour appears to be not ideal, it enables analysing a region often discarded in physics analyses. As demonstrated in this work, it is possible to probe the entire mass region via a unified approach.

The above tests do not rely on any signal hypotheses, as the statistical analysis aims at identifying significant deviations in data without analysing the nature of the deviations or quantifying the size of the potential BSM signals. This model-agnostic approach has its merits in many occasions, such as analyses designed with minimal BSM assumptions. However, the ability to extract the signal component is still very much demanded. It is possible to achieve this goal as suggested by the authors of ref. [25], using a stationary kernel, S , to model the signal component:

$$S = A \exp^{-\frac{1}{2}(x_i - x_j)^2 / l_s^2} \exp^{-\frac{1}{2}((x_i - m)^2 + (x_j - m)^2) / t^2}$$

where A is a constant, l_s refers to the length scale, m specifies the centre of the signal mass, and t acts as the width of the signal [25]. Therefore, the full GPR model becomes $S + C(c) \times \text{RBF}(\ell)$. The bound of the length scale of the background kernel, l_0 (l_1), is set to be 0.6(0.7), determined by the background only tests. The hyperparameters associated with the signal kernel are determined by fitting the signal templates. While both A and l_s can float freely, m and t are only allowed to change within a reasonable range of the fitted values. Given the logarithmic transformation done to the dataset in Section 3.1, the signal in the original space is approximated by $\exp^{s+b} - \exp^b$, where s and b are the signal and background components obtained via the fitted kernels. Figure 9 shows the signal extraction results for the 800 GeV gaussian-like signal with a 5% width. The number of extracted signal increases as the amount of injected signal events, roughly following a linear response. However, the extracted signal strength is systematically higher and has a wide spread. The performance of signal extraction becomes very unstable for signal points close to the m_{jj} boundaries. The data pre-processing, kernel selection and hyperparameters all affect the signal extraction performance, which can be further optimised. We use this example to demonstrate there exists a viable strategy.

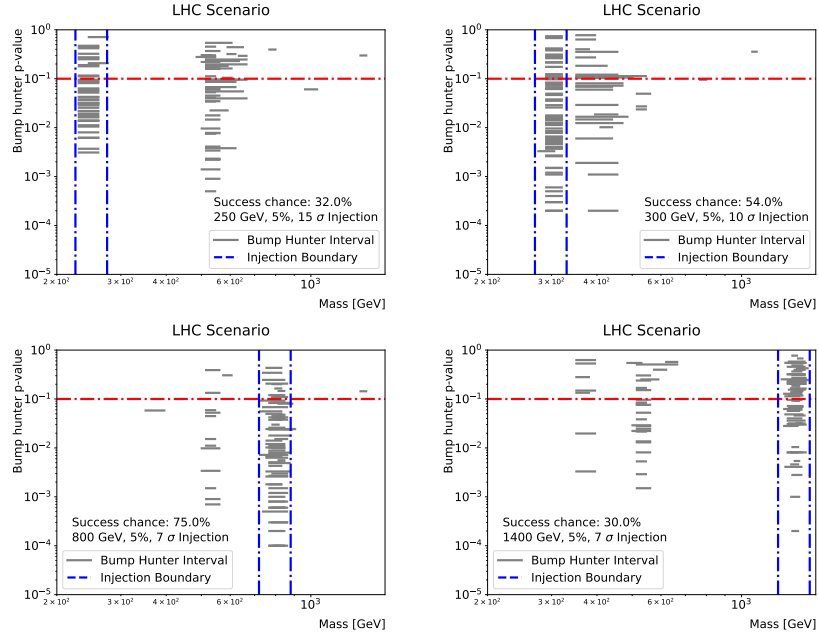


Figure 7: Summary of the BH p -values and the corresponding mass intervals (solid horizontal segment), for the 250 GeV (upper-left), 300 GeV (upper-right), 800 GeV (lower-left) and 1400 GeV (lower-right) signal mass points. The horizontal dashed line corresponds to a critical value of 0.1.

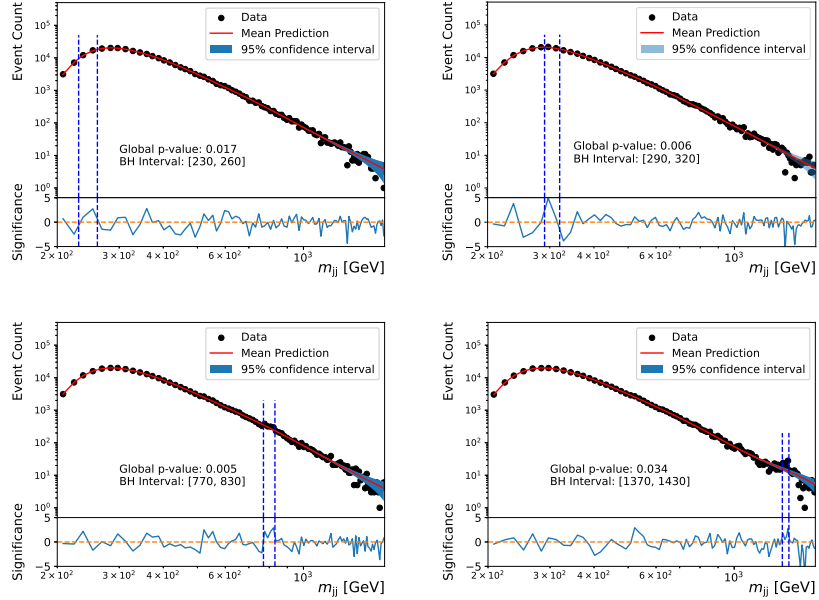


Figure 8: Comparison between the signal-injected pseudo-dataset (solid point) and the background estimate from GPR (solid line), for the 250 GeV (upper-left), 300 GeV (upper-right), 800 GeV (lower-left) and 1400 GeV (lower-right) signal mass points. The vertical dashed lines indicate the boundaries of the most significant deviation reported by BH.

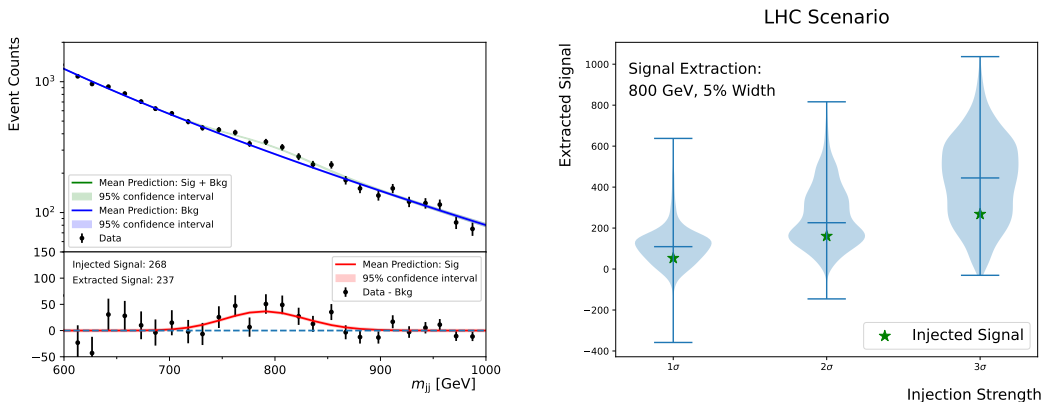


Figure 9: An example of signal extraction test done for the 800 GeV gaussian-like signal with a 5% width (left), and the summary of test results with different injected signal strengths (right). The numbers of injected signal events are indicated by the green stars, while the blue crosses represent the medians of extracted signal.

6 Robustness in HL-LHC

The authors of ref. [25] conducted a test showing that the GPR-based background estimate has a stable χ^2 result as the luminosity increases. Here, we extend this study to also include the KS and BH tests, in the HL-LHC condition. The analysis done in ref. [30] uses 36.1 fb^{-1} of data, which is only 1.2% of the total integrated luminosity expected for HL-LHC. As a consequence, events at the high m_{jj} tail expected in HL-LHC have not been collected in this dataset. In order to obtain a test dataset that corresponds to the HL-LHC scenario, the following procedure is applied:

- Fit the 36.1 fb^{-1} m_{jj} spectrum obtained by GPR using $f(x) = p_0(1-x)^{p_1}x^{p_2}$, where $x = m_{jj}/6500$, starting from $m_{jj} = 1000 \text{ GeV}$.
- Use the fitted function to predict the yields at high mass tail that is not available in the 36.1 fb^{-1} dataset.
- Scale the whole spectrum, to the target integrated luminosity at the HL-LHC, which is 3000 fb^{-1} .

Figure 10 shows the template used to generate the pseudo-datasets for the HL-LHC scenario and one example dataset. It is acknowledged that the events at the high mass tail may not accurately represent the real data to be collected, but it suits the scope of this study, which is to check the robustness of GPR against increasing luminosity.

The same set of tests are performed using the above pseudo-datasets. Since the mass region is enlarged by a factor of 2.5 compared to the LHC test dataset, the widest window considered in BH is increased by a factor of 2 [34, 35]. We only observe weak biases in the BH p -value test, as shown in Figure 11. The results from KS and χ^2 tests are also very similar.

Since the mass region is extended up to 4 TeV given the expected HL-LHC luminosity, the 800 GeV and 1400 GeV signal mass points are changed to 2000 GeV and 3400 GeV, respectively, for the signal injection tests. The resulting BH p -values are shown in Figure 12, which are similar to the LHC scenario.

However, BH fails to report the most significant deviations at the correct location when the 300 GeV signal is injected, although the fraction of BH p -values below 0.1 is high, as shown in Figure 13. It is already observed in the LHC scenario, but the impact is enhanced due to a much larger luminosity. Figure 14 shows random examples of the pseudo-experiments that have successfully reported a p -value below 0.1, with the BH intervals marked as well.

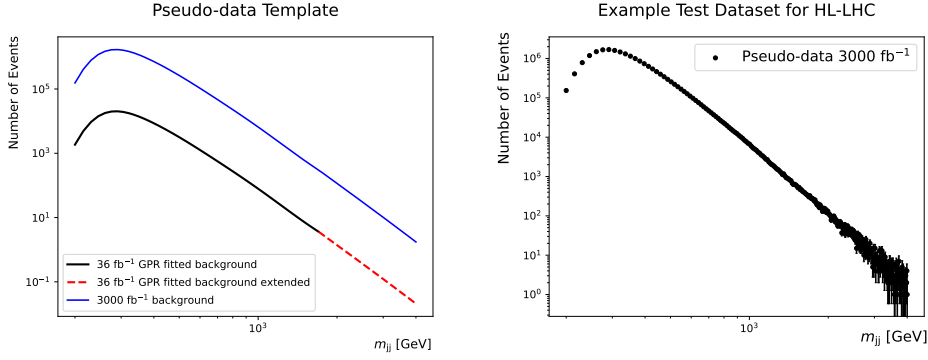


Figure 10: The smooth template used to generate pseudo-dataset (left) and one of the example pseudo-datasets (right), representing the HL-LHC scenario.

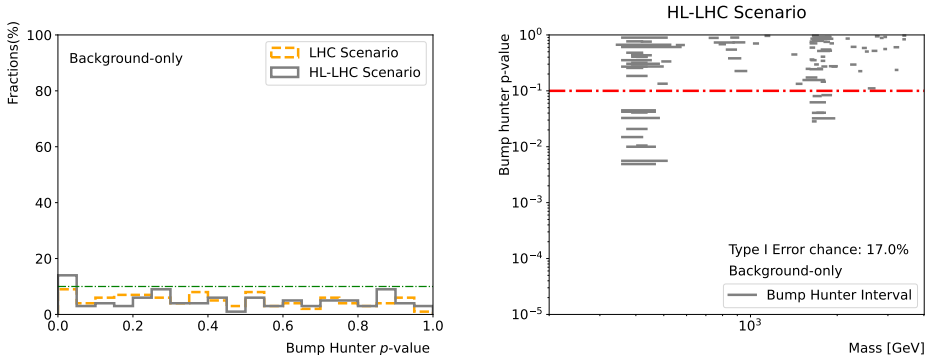


Figure 11: Left: BH p -value distributions of 100 background-only pseudo-experiments in the HL-LHC condition (solid line). Right: a summary of the BH p -values and the corresponding mass intervals (horizontal solid segments).

The same signal extraction procedure is tested for the HL-LHC scenario as well, using the 2000 GeV gaussian-like signal with a 5% width. The performance is similar to that of the LHC scenario. The signal extraction is systematically higher, with a wide spread.

The overall performance of the same GPR model decreases slightly in the HL-LHC scenario if the hyperparameters are not re-optimised (HL-LHC results using re-optimised hyperparameters are discussed in Appendix A.). It is remarkable as the luminosity is increased by a magnitude of two. The hyperparameters allow the users to tune the model with great flexibility, while the traditional functional fit method limits the users to a given function family. Due to the sizeable correlations between the free parameters, the fit performance of a function is saturated after reaching a certain number of free parameters. In contrast, the GPR-based background modelling technique can offer a solution that is valid through the entire lifetime of the LHC.

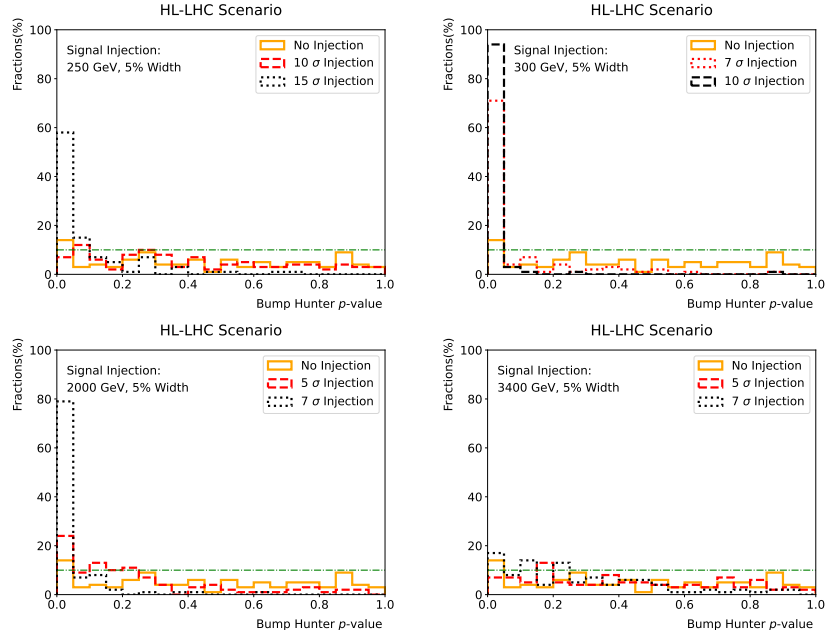


Figure 12: Summary of BH p -values obtained in the signal injection tests in the HL-LHC condition, for the 250 GeV (upper-left), 300 GeV (upper-right), 2000 GeV (lower-left) and 3400 GeV (lower-right) signal mass points.

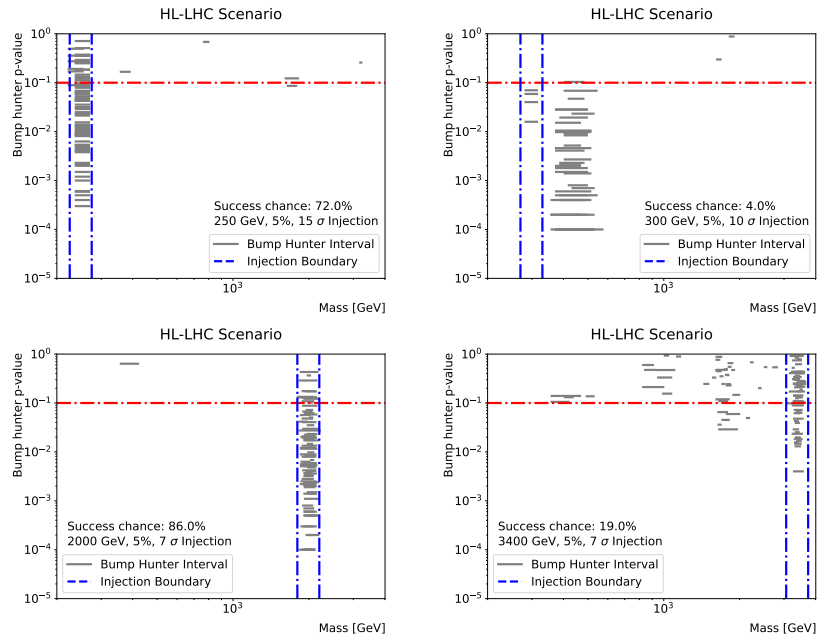


Figure 13: Summary of the BH p -values and the corresponding mass intervals (solid horizontal segment), for the 250 GeV (upper-left), 300 GeV (upper-right), 2000 GeV (lower-left) and 3400 GeV (lower-right) signal mass points, in the HL-LHC condition. The horizontal dashed line corresponds to a critical value of 0.1.

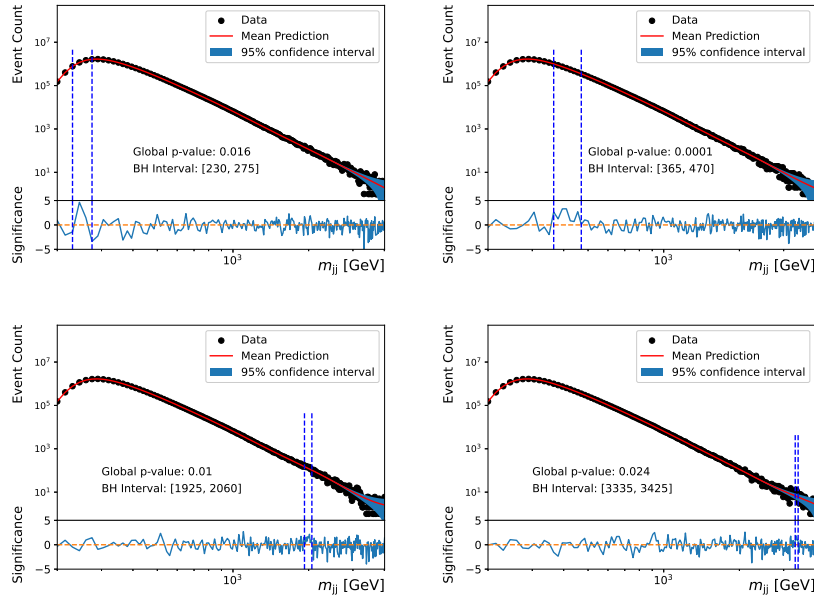


Figure 14: Comparison between the signal-injected pseudo-data (solid point) and the background estimate from GPR (solid line), for the 250 GeV (upper-left), 300 GeV (upper-right), 2000 GeV (lower-left) and 3400 GeV (lower-right) signal mass points, in the HL-LHC condition. The vertical dashed lines indicate the boundaries of the most significant deviation reported by BH.

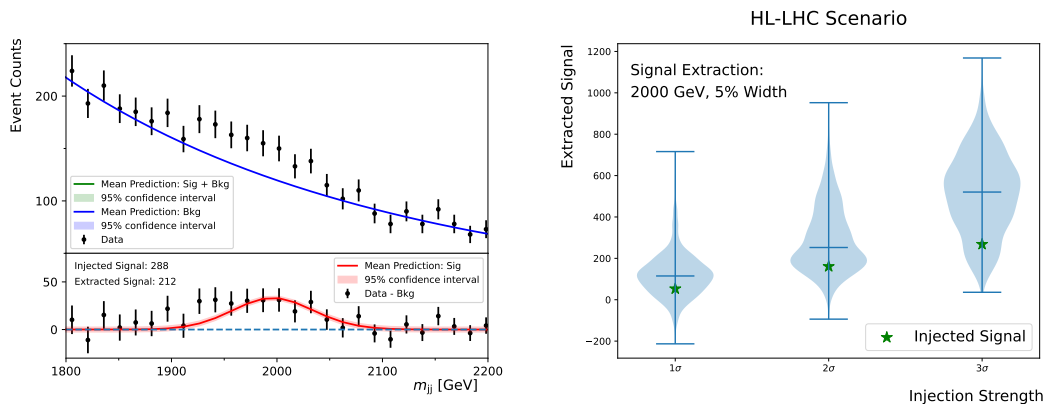


Figure 15: An example of signal extraction test done for the 2000 GeV gaussian-like signal with a 5% width (left), and the summary of test results with different injected signal strengths (right). The numbers of injected signal events are indicated by the green stars, while the blue crosses represent the medians of extracted signal.

7 Summary

In this work, the performance of a GPR-based background estimation method is thoroughly investigated, with a set of tests performed using a background spectrum reported in a CMS search [30]. The background is challenging as it also includes the region before the smoothly falling part. The CMS search divides the background into three separate regions, with each fitted by a different function. Owing to the flexible nature of GPR, this delicate spectrum can be handled in a much simpler way. We point out that one can rely on the most commonly adopted RBF kernel to achieve excellent performance if the L_2 regularisation is tuned accordingly. Thus, for a GPR-based background estimate model, the set of hyperparameters includes the bounds of the kernel parameters and the regularisation matrix. The discovery potential is evaluated using the BUMPHUNTER algorithm [34]. With a minimally optimised set of hyperparameters, we observe promising sensitivity to hypothetical narrow resonances. In addition, the background is projected to the HL-LHC to test how robust GPR is against increasing luminosity. Unlike traditional functional fit methods that have already been challenged seriously during Run 2, the performance of the GPR-based strategy is remarkably stable even for the HL-LHC scenario. The signal extraction procedure is tested as well, without optimisation for this specific task. While the outcome is positive, it is obvious that the performance should be improved. An automatic and systematic way to tune a GPR-based model to suit all major use cases is of high value, which is an interesting topic for future studies.

Recent LHC analyses have started experimenting with GPR on various occasions [16, 28, 29], but functional fit is still the most widely embraced method in resonance searches. It is in part due to its long historical success, and there are well-established procedures to address topics such as systematic uncertainties and to integrate it into the statistical analysis [36]. In this work, we illustrate that GPR can satisfy the common standards imposed for searches using the BUMPHUNTER algorithm, even if a very difficult background shape is under consideration. Tuning the hyperparameters in a GPR model is conceptually. It is clear that GPR is already suitable for certain types of searches at the LHC, and we look forward to more results adopting this method. Its robustness against increasing luminosity allows the community to develop background estimate strategies that are valid throughout the entire lifetime of the (HL)-LHC. It is not discussed here how to evaluate the major systematic uncertainties associated with GPR and how the hyperparameters can impact them. We leave this topic for future works.

Acknowledgments

GPR-based methods have been investigated by the ATLAS collaboration for several years. We have learned a lot from numerous talks given by our colleagues, and those pioneering GPR applications in ATLAS analyses. We thank Rachel Hyneman for helping with the signal extraction workflow, and Marco Montella for valuable suggestions. Jackson B. is supported by the STFC UCL Centre for Doctoral Training in Data Intensive Science (grant ST/P006736/1), including by departmental and industry contributions. B.X. Liu is supported by Shenzhen Campus of the Sun Yat-sen University under project 74140-12240013. B.X. Liu appreciates the support from Guangdong Provincial Key Laboratory of Gamma-Gamma Collider and Its Comprehensive Applications, and the support from Guangdong Provincial Key Laboratory of Advanced Particle Detection Technology.

Appendix

A Impacts of the L_2 regularisation

In the HL-LHC scenario, it is observed that the background modelling biases are increased as shown in Figure 11. Consequently, a large fraction of most significant BH-intervals being reported at the wrong locations when the 300 GeV signal events are injected, as reported by Figure 12. As mentioned in Section 3.3, the multiplication factor f_i can serve as a set of hyperparameters. In this appendix, we

demonstrate that tuning f_i helps with achieving better background modelling performance for the HL-LHC scenario.

Both Figure 11 and Figure 12 indicate that the background modelling is sub-optimal around 400 GeV. Therefore, we modify the corresponding f_i to enhance the performance in this region. The original $f_{1-11} = 0.1$ is updated to $f_{1-20} = 0.1$. Figure A.1 compares the BH p -values obtained in the background-only tests and the BH intervals reported using the updated multiplication factor. The systematic pattern seen around 400 GeV before is greatly mitigated as expected. Figure A.2 compares the 300 GeV signal injection test results using the original ($f_{1-11} = 0.1$) and re-tuned $f_{1-20} = 0.1$. The latter correctly reports the excess at the location where the signal events are injected.

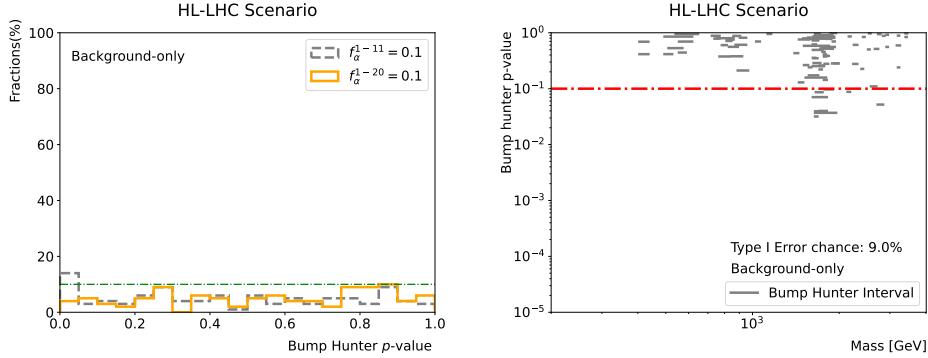


Figure A.1: Left: BH p -value comparison between results using original tuned hyperparameters ($f_{1-11} = 0.1$) and the ones using re-tuned hyperparameters ($f_{1-20} = 0.1$), for the HL-LHC scenario. Right: summary of the BH p -values and the corresponding mass intervals (solid horizontal segment), for the background-only tests, in the HL-LHC condition.

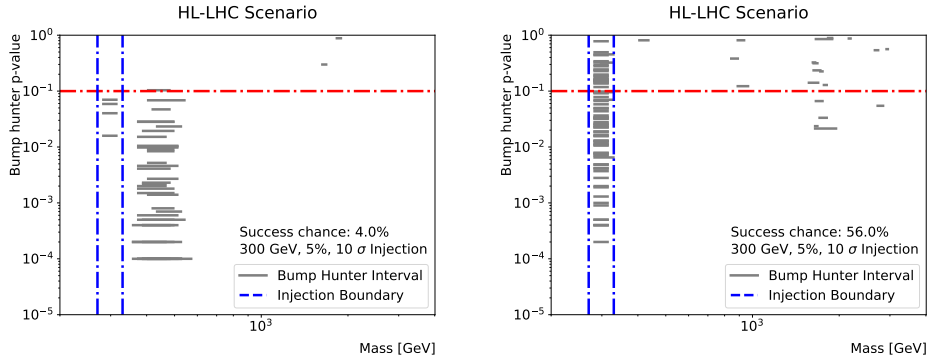


Figure A.2: Comparisons of the BH p -values and the corresponding mass intervals between results using original tuned hyperparameters ($f_{1-11} = 0.1$) and the ones using re-tuned hyperparameters ($f_{1-20} = 0.1$), for the 300 GeV signal injection test, in the HL-LHC condition.

This exercise demonstrates that the L_2 regularization has significant impact on the background modelling performance. Tuning the corresponding hyperparameters allows to adapt the GPR model to various new conditions easily.

Bibliography

- [1] ATLAS Collaboration. Exploration at the high-energy frontier: ATLAS Run 2 searches investigating the exotic jungle beyond the Standard Model. 3 2024, 2403.09292.

- [2] CMS Collaboration. Dark sector searches with the CMS experiment. 5 2024, 2405.13778.
- [3] CMS Collaboration. Enriching the Physics Program of the CMS Experiment via Data Scouting and Data Parking. 3 2024, 2403.16134.
- [4] ATLAS Collaboration. Electroweak, QCD and flavour physics studies with ATLAS data from Run 2 of the LHC. 4 2024, 2404.06829.
- [5] ATLAS Collaboration. Climbing to the Top of the ATLAS 13 TeV data. 4 2024, 2404.10674.
- [6] Simone Alioli, Keith Hamilton, Paolo Nason, Carlo Oleari, and Emanuele Re. Jet pair production in POWHEG. *JHEP*, 04:081, 2011, 1012.3380.
- [7] Adam Kardos, Paolo Nason, and Carlo Oleari. Three-jet production in POWHEG. *JHEP*, 04:043, 2014, 1402.4001.
- [8] Simone Alioli, Paolo Nason, Carlo Oleari, and Emanuele Re. A general framework for implementing NLO calculations in shower Monte Carlo programs: the POWHEG BOX. *JHEP*, 06:043, 2010, 1002.2581.
- [9] Torbjörn Sjöstrand, Stefan Ask, Jesper R. Christiansen, Richard Corke, Nishita Desai, Philip Ilten, Stephen Mrenna, Stefan Prestel, Christine O. Rasmussen, and Peter Z. Skands. An introduction to PYTHIA 8.2. *Comput. Phys. Commun.*, 191:159–177, 2015, 1410.3012.
- [10] Rikkert Frederix, Stefano Frixione, Valentin Hirschi, Davide Pagani, Hua-Sheng Shao, and Marco Zaro. The complete NLO corrections to dijet hadroproduction. *JHEP*, 04:076, 2017, 1612.06548.
- [11] CMS Collaboration. Azimuthal correlations for inclusive 2-jet, 3-jet, and 4-jet events in pp collisions at $\sqrt{s} = 13$ TeV. *Eur. Phys. J. C*, 78(7):566, 2018, 1712.05471.
- [12] ATLAS Collaboration. Measurement of the inclusive jet cross-section in proton-proton collisions at $\sqrt{s} = 7$ TeV using 4.5 fb^{-1} of data with the ATLAS detector. *JHEP*, 02:153, 2015, 1410.8857. [Erratum: *JHEP* 09, 141 (2015)].
- [13] Michal Czakon, Alexander Mitov, and Rene Poncelet. Next-to-Next-to-Leading Order Study of Three-Jet Production at the LHC. *Phys. Rev. Lett.*, 127(15):152001, 2021, 2106.05331. [Erratum: *Phys.Rev.Lett.* 129, 119901 (2022)].
- [14] ATLAS Collaboration. Search for new resonances in mass distributions of jet pairs using 139 fb^{-1} of pp collisions at $\sqrt{s} = 13$ TeV with the ATLAS detector. *JHEP*, 03:145, 2020, 1910.08447.
- [15] ATLAS Collaboration. Search for low-mass dijet resonances using trigger-level jets with the ATLAS detector in pp collisions at $\sqrt{s} = 13$ TeV. *Phys. Rev. Lett.*, 121(8):081801, 2018, 1804.03496.
- [16] CMS Collaboration. Searches for Pair-Produced Multijet Resonances using Data Scouting in Proton-Proton Collisions at $\sqrt{s} = 13$ TeV. *Phys. Rev. Lett.*, 133(20):201803, 2024, 2404.02992.
- [17] ATLAS Collaboration. Search for resonances decaying into photon pairs in 139 fb^{-1} of pp collisions at $\sqrt{s}=13$ TeV with the ATLAS detector. *Phys. Lett. B*, 822:136651, 2021, 2102.13405.
- [18] UA2 Collaboration. A Study of multi-jet events at the CERN anti-p p collider and a search for double parton scattering. *Phys. Lett. B*, 268:145–154, 1991.
- [19] UA2 Collaboration. A Search for new intermediate vector mesons and excited quarks decaying to two jets at the CERN $\bar{p}p$ collider. *Nucl. Phys. B*, 400:3–24, 1993.
- [20] CMS Collaboration. Measurements of Higgs boson production cross sections and couplings in the diphoton decay channel at $\sqrt{s} = 13$ TeV. *JHEP*, 07:027, 2021, 2103.06956.
- [21] Ryan Edgar, Dante Amidei, Christopher Grud, and Karishma Sekhon. Functional Decomposition: A new method for search and limit setting. 5 2018, 1805.04536.
- [22] ATLAS Collaboration. Search for heavy particles in the b -tagged dijet mass distribution with additional b -tagged jets in proton-proton collisions at $\sqrt{s}= 13$ TeV with the ATLAS experiment. *Phys. Rev. D*, 105(1):012001, 2022, 2108.09059.
- [23] Ho Fung Tsoi, Dylan Rankin, Cecile Caillol, Miles Cranmer, Sridhara Dasu, Javier Duarte, Philip Harris, Elliot Lipeles, and Vladimir Loncar. SymbolFit: Automatic Parametric Modeling with

Symbolic Regression. 11 2024, 2411.09851.

- [24] Carl Edward Rasmussen and Christopher K. I. Williams. *Gaussian Processes for Machine Learning*. The MIT Press, 55 Hayward St, Cambridge, MA 02142, 2006.
- [25] Meghan Frate, Kyle Cranmer, Saarik Kalia, Alexander Vandenberg-Rodes, and Daniel Whiteson. Modeling Smooth Backgrounds and Generic Localized Signals with Gaussian Processes. 9 2017, 1709.05681.
- [26] Abhijith Gandrakota, Amit Lath, Alexandre V. Morozov, and Sindhu Murthy. Model selection and signal extraction using Gaussian Process regression. *JHEP*, 02:230, 2023, 2202.05856.
- [27] ATLAS Collaboration. Search for boosted diphoton resonances in the 10 to 70 gev mass range using 138 fb^{-1} of 13 tev pp collisions with the atlas detector. *Journal of High Energy Physics*, 2023(7):155, 2023.
- [28] ATLAS Collaboration. Search for boosted diphoton resonances in the 10 to 70 GeV mass range using 138 fb^{-1} of 13 TeV pp collisions with the ATLAS detector. *JHEP*, 07:155, 2023, 2211.04172.
- [29] ATLAS Collaboration. Search for the associated production of charm quarks and a Higgs boson decaying into a photon pair with the ATLAS detector. *JHEP*, 02:045, 2025, 2407.15550.
- [30] CMS Collaboration. Search for beyond the standard model Higgs bosons decaying into a $b\bar{b}$ pair in pp collisions at $\sqrt{s} = 13 \text{ TeV}$. *JHEP*, 08:113, 2018, 1805.12191.
- [31] Andrew Ng. Feature selection, l_1 vs. l_2 regularization, and rotational invariance. *Proceedings of the Twenty-First International Conference on Machine Learning*, 09 2004.
- [32] Karl Pearson. X. on the criterion that a given system of deviations from the probable in the case of a correlated system of variables is such that it can be reasonably supposed to have arisen from random sampling. *The London, Edinburgh, and Dublin Philosophical Magazine and Journal of Science*, 50(302):157–175, July 1900.
- [33] Frank J. Massey. The kolmogorov-smirnov test for goodness of fit. *Journal of the American Statistical Association*, 46:68–78, 1951.
- [34] Georgios Choudalakis. On hypothesis testing, trials factor, hypertests and the BumpHunter. In *PHYSTAT 2011*, 1 2011, 1101.0390.
- [35] Louis Vaslin, Samuel Calvet, Vincent Barra, and Julien Donini. pyBumpHunter: A model independent bump hunting tool in Python for High Energy Physics analyses. *SciPost Phys. Codeb.*, 2023:15, 2023, 2208.14760.
- [36] ATLAS Collaboration. Recommendations for the Modeling of Smooth Backgrounds. 2020.